Article

Size and Structural Dependence of Cohesive Energy in Cu

W. Liu, D. Liu, W. T. Zheng, and Q. Jiang

More About This Article

Additional resources and features associated with this article are available within the HTML version:

- Supporting Information
- Access to high resolution figures
- Links to articles and content related to this article
- Copyright permission to reproduce figures and/or text from this article

View the Full Text HTML

Size and Structural Dependence of Cohesive Energy in Cu

W. Liu, D. Liu, W. T. Zheng, and Q. Jiang*

Key Laboratory of Automobile Materials, Ministry of Education, and Department of Materials Science and Engineering, Jilin University, Renmin Street 5988, Changchun 130022, China

The cohesive energy of Cu clusters (E_c) containing different numbers of atoms (n) in the metastable structures of pyramids, nanotubes, nanorods, films, and icosahedrons is determined using ab initio density functional theory (DFT). Modeling of $E_c(n)$ functions is also implemented and discussed. Both theoretical and simulation results show that $E_c(n)$ is a function of the surface bond deficit, and $E_c(n)$ increases monotonically as n decreases, as follows: $E_{cNanotube}(n) > E_{cPyramid}(n) > E_{cIcosahedron}(n) > E_{cNanorod}(n) > E_{cFilm}(n)$ for a given n. This observed continuity of the $E_c(n)$ functions implies that the quantum effect of $E_c(n < n_c)$ is not influenced by n or a size effect but instead by a structural effect, where n_c denotes a critical value of n when the bulk crystalline structure is no longer stable for $n < n_c$. This suggestion is in good agreement with the results obtained from the observed distributions of the density of states (DOS).

1. Introduction

Clusters are defined as building blocks of 10^1 to 10^6 atoms or molecules,[1] specified by substantial differences in physical, chemical, and mechanical properties as compared to those of the counterpart bulk materials.[2−5] Such properties are determined by the corresponding cohesive energies $E_c(n)$, where n denotes the number of atoms in the clusters.[6] It has been demonstrated that the crystalline structure is stable when n is larger than a critical size, such as $n_c \sim 10^3 - 10^4$. This results in the increase of $E_c(n > n_c)$ with a monotonic decrease in n, indicating a proportional relationship of the surface/volume ratio δ.[7,8] The theoretically predicted $E_c(n)$ function is in good agreement with experimental results reported in the literature.[8,9] The $E_c(n)$ function can also be extended to estimate other properties, such as surface energy γ, melting temperature, Curie transition temperature, Debye temperature, diffusion activation energy, and vacancy formation energy.[10,11] However, the clusters may be polymorphic when $n < n_c$.[12] For example, the equilibrium isomers of Au, Ag, Cu, and Ni with $2 < n < 150$ predominantly consist of icosahedrons with islands of face-centered cubic (fcc), tetrahedrons, and decahedrons, while their bulk structures are fcc.[13,14] The sequential growth of Cu clusters demonstrates structural changes from triangle to icosahedron and finally to fcc.[3] As a result, the corresponding $E_c(n)$ function is no longer monotonic. It was reported that $-E_c(n) = 2.83, 2.96, 2.93, 3.07, 3.05,$ and 3.07 eV/atom for $n = 7,8,...,12$ as calculated by density functional theory (DFT),[11] while the hybridization between Cu-3d and Cu-4s orbitals with $n = 8−20$ has a limited influence on the cluster shape.[2] Conversely, for Au clusters, $E_c(\text{even } n) < E_c(n − 1)$[15] due to the variation in the number of broken bonds B_b and δ of the clusters.[16]

The results discussed above demonstrate that the size effect on $E_c(n > n_c)$ is a function of δ ($\delta < 0.5$) and that it plays an important role in determining the cluster structures,[8] whereas the influence of δ on $E_c(n < n_c)$ is limited as $\delta \rightarrow 1$. Theoretical studies suggest that the variation of $E_c(n > n_c)$ and $E_c(n < n_c)$ near the critical number of atoms n_c is different, and further

examination of the scientific literature shows that in depth studies of the size dependence of E_c for the case of $n < n_c$ are not available. Studying the size effects on $E_c(n < n_c)$ will provide new insights into fundamental understandings of the physical properties of nanoclusters, as well as their surface behavior under the extreme conditions, such as those associated with $\delta \rightarrow 1$. To establish a universal model to describe this physical phenomenon, the polymorphism of the clusters should also be considered. As $\delta \rightarrow 1$, the variation of δ with respect to the change of n is minimal, and the effect of the bulk surface energy γ is not significant on cluster structures. In this case, a new variant should be used in the establishment of the $E_c(n)$ function, which is associated with the surface bond deficit Z_s/Z_b, where Z_s denotes the mean coordination number (CN) of surface atoms and Z_b indicates the CN in the bulk material. However, the appropriate substitution of δ should be B_a/B_t, where $B_a = B_t − B_b$ is the rest bond number and B_t denotes the total bond number in a system. The relationship among $E_c(n)$, δ, Z_s/Z_b, and B_a/B_t could be clarified during the development of the theoretical $E_c(n)$ function. In conjunction with investigating the atomic and electronic structures of the clusters, computer simulations can be effectively used to validate the accuracy of the modeling.

In this work, five size-independent structures of Cu clusters are established. $E_c(n < n_c)$ functions of these structures are determined from both macroscopic and microscopic frameworks. The former is on the basis of classic energetic theory with geometric consideration, while the latter is obtained by DFT calculations. The results obtained are used to compare the calculation consequence using δ, Z_s/Z_b, and B_a/B_t as variants. In addition, the corresponding electronic structures are determined to support the obtained $E_c(n)$ functions in electronic aspects.

2. Calculation Details and Modeling

2.1. DFT Calculations. All DFT calculations are implemented in DMol^3 code.[17,18] GGA-RPBE (Revised-Perdew−Burke−Ernzerhof) was employed as the exchange-correlation function.[19] The RPBE function is advantageous in the calculation of energies for small molecules because it attains

---

　* Author to whom correspondence should be addressed. Fax: +86 431 85095876. E-mail: Jiangq@jlu.edu.cn.

Size and Structural Dependence of E_c in Cu

J. Phys. Chem. C, Vol. 112, No. 48, 2008 **18841**
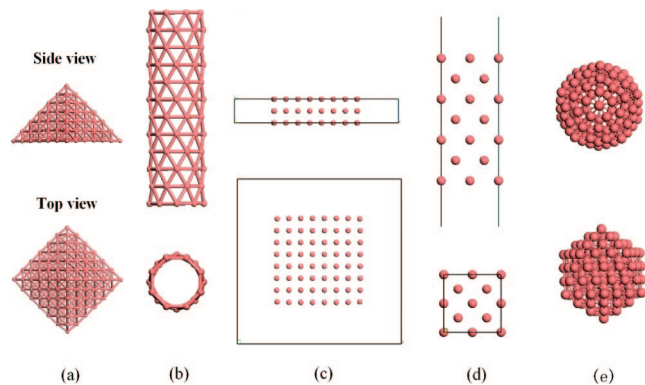
Figure 1. Structures of Cu clusters: (a) pyramids, (b) nanotubes, (c) nanorods, (d) films, and (e) icosahedrons.

a significantly reduced mean absolute error in molecular atomization energies.[20] Spin polarization is introduced by the unpaired 4s electron in Cu atoms. DFT semicore pseudopotentials (DSPP) were employed to replace the core electron potentials by a single effective potential, while also accounting for relativistic effects.[21] In the pseudopotential approach, the highest s and d states of the transition metals are usually treated as valence states, while the core orbitals are often approximated as unaffected by a change in the environment. Since the electronic configuration of Cu is $[Ar]3d^{10}4s^1$, the Cu-3d and Cu-4s are treated as the valence states, while the inner orbitals are done as core in our calculations. Additionally, DNP was chosen as the basis set, which uses double-numeric basis with polarization functions, i.e., functions with angular momentum, one being higher than that of the highest occupied orbital in free atoms.[17] For each structure, the SCF tolerance was set at 1.0×10^{-5}, with max SCF cycles of 1000 and a smearing of 0.005 Ha (1 Ha = 27.2114 eV).

Five configurations of cluster structures, pyramids, single-wall nanotubes, nanorods, thin films, and icosahedrons with different n and δ values were constructed and shown in Figure 1. Their dimensions are $d = 0, 1, 1, 2$, and 0, respectively. Note that n values of the nanorod and the film are infinite in one and two dimensions, respectively (although only finite segments of these structures are given in Figure 1). To ensure that the interaction between the periodically repeated cells along the normal of the surface is small, both x and y directions of the nanorods are constrained by a 12 Å vacuum.[22] Similarly, a vacuum thickness of 12 Å is employed along the z direction of the (2×2) Cu(100) films. The k-points used in the Brillioun zone integration are set to $1 \times 1 \times 8$ mesh for the nanorods and $5 \times 5 \times 1$ for the films which have been demonstrated to be suitable for the film calculations.[22] These settings present a convergence tolerance of energy of 2.0×10^{-5} Ha, a maximum force of 0.004 Ha/Å, and a maximum displacement of 0.005 Å. All atoms in each cluster were allowed to relax without any constraining under the premises that the set structure remains.

The E_c is an important physical parameter to estimate the strength of metallic bonds, which equals the energy that can divide the metal into isolated atoms by destroying all metallic bonds.[6,23] In simulation, the $E_c(n)$ value per atom is given by[24]

$$E_c(n) = (E_{cluster} - nE_{atom})/n \qquad (1)$$

where $E_{cluster}$ and E_{atom} are the total energy of a Cu cluster and a single Cu atom, respectively. Note that the unit of E_c is in eV/atom. Two boundary conditions are $E_c(n = 1) = 0$ and $E_c(n \rightarrow \infty) \approx E_{cBulk}$ where the subscript Bulk denotes the bulk size.

2.2. Theoretical Models. The established five structures represent different structure characteristics with distinct d and δ values. For these structures, $B_t = Z_b n/2$, where $Z_b = 12$. Thus

$$B_t = 6n \qquad (2)$$

B_a is structure-dependent. As shown in Figure 1a, the pyramid with the symmetry of C_{4v} is an equilateral triangle from the side view and a square from the top view. All five surfaces consist of close-packed atoms, $1 \leq l \leq 7$, where l is the layer number. $\delta = 1$ when $1 \leq l \leq 3$ and $\delta = 1 - [1 + 2^2 + ... (l - 3)^2]/(1 + 2^2 + ... + l^2)$ at $4 \leq l \leq 7$. When $l > 1$, $n_{uv} = 1$, $n_{bv} = 4$, $n_{le} = n_{be} = 4(l - 2)$, $n_{lf} = 2(l^2 - 5l + 6)$, $n_{bf} = (l - 2)^2$, and $n_i = (2l^3 - 15l^2 + 37l - 30)/6$ where the subscripts denote the atoms at the uppermost vertex, bottom vertices, lateral edges, bottom edges, lateral facets, bottom facets, and interior, respectively. $n_{sPyramid} = 3l^2 - 6l + 5$ and $n_{Pyramid} = (2l^3 + 3l^2 + l)/6$ where the subscript s denotes the surface. CN of the surface atoms at different locations are deduced as $Z_{uv} = 4$, $Z_{bv} = 3$, $Z_{le} = 7$, $Z_{be} = 5$, $Z_{lf} = 9$, and $Z_{bf} = 8$. $Z_{sPyramid}$ and $B_{aPyramid}$ are given as

$$Z_{sPyramid} = (4n_{uv} + 3n_{bv} + 7n_{le} + 5n_{be} + 9n_{lf} + 8n_{bf})/n_{sPyramid} \qquad (3.1a)$$

$$B_{aPyramid} = (4n_{uv} + 3n_{bv} + 7n_{le} + 5n_{be} + 9n_{lf} + 8n_{bf} + 12n_i)/2 \qquad (3.1b)$$

The nanotube shown in Figure 1b has a symmetry group of D_{4h}. Each circle consists of eight atoms as viewed from the top, with a stacking sequence of ABAB. The largest length of the nanotube is about 2.34 nm and $2 \leq l \leq 12$ with $\delta \equiv 1$. Since the nanotube has a curved facet, the surface atoms should have different CN from that of a plane facet, with $n_e = 16$ and $n_f = 8(l - 2)$. The atoms on a curved facet can be approximated as edge atoms intersected by two (111) planes in our case, and its CN should be 7. Thus, $Z_f = 7$ and $Z_e = 5$, where subscripts f and e denote atoms at the facet and the edge. $n_{sNanotube} = n_{Nanotube} = 8l$. $Z_{sNanotube}$ and $B_{aNanotube}$ are shown as

$$Z_{sNanotube} = (5n_e + 7n_f)/8l \qquad (3.2a)$$

$$B_{aNanotube} = (5n_e + 7n_f)/2 \qquad (3.2b)$$

The widths of nanorods shown in Figure 1c increase from (2×2) to (8×8) with $2 \leq l \leq 8$, $Z_e = 5$, and $Z_f = 8$,[22] resulting in $\delta = 1 - (l - 2)^2/l^2$ at $2 \leq l \leq 8$. $n_e = 4$, $n_f = 4(l - 2)$, and $n_i = (l - 2)^2$. $n_{sNanorod} = 4(l - 1)$, and $n_{Nanorod} = l^2$. $Z_{sNanorod}$ and $B_{aNanorod}$ are given as

$$Z_{sNanorod} = (5n_e + 8n_f)/[4(l - 1)] \qquad (3.3a)$$

$$B_{aNanorod} = (5n_e + 8n_f + 12n_i)/2 \qquad (3.3b)$$

The l values of Cu(100) films shown in Figure 1d increase from 2 to 12, and the maximum thickness is about 2.10 nm along the z axis. $\delta = 2/l$, $n_{Film} = 4l$, $n_f = 8$, and $n_i = 4(l - 2)$. Z_{sFilm} and B_{aFilm} are given as

$$Z_{sFilm} = Z_f = 8 \qquad (3.4a)$$

$$B_{aFilm} = 4n_f + 24(l - 2) \qquad (3.4b)$$

The icosahedral clusters in Figure 1e demonstrate a quasi-spherical shape and a close-packed surface with 20 distorted (111)-like close-packed facets, thus optimizing the surface energy well.[25] This indicates that icosahedra can potentially be the most favorable structure at small sizes.[26] In this work, three icosahedra are considered with $n = 13, 55$, and 147. $n_v = 12$, $n_e = 30(l - 2)$, $n_f = 10(l^2 - 5l + 6)$, and $n_i = 10l^3/3 - 15l^2$

+ $71l/3 - 13$ where v, e, f, and i separately denote the atoms at vertex, edge, facet, and inner sites of the cluster. $n_{sIcosahedron} = 10l^2 - 20l + 12$, $Z_v = 6$, $Z_e = 8$, $Z_f = 9$, and $Z_i = 12$. $Z_{sIcosahedron}$ and $B_{aIcosahedron}$ are given as

$$Z_{sIcosahedron} = (6n_V + 8n_e + 9n_f)/n_{sIcosahedron} \quad (3.5a)$$

$$B_{aIcosahedron} = (6n_V + 8n_e + 9n_f + 12n_i)/2 \quad (3.5b)$$

$E_c(n)$ can be determined by an energetic sum of the surface and interior with

$$E_c(n) = \delta(E_{cBulk} + \gamma) + (1 - \delta)E_{cBulk} \text{ or } E_c(n)/E_{cBulk} = 1 + \gamma\delta/E_{cBulk} \quad (4)$$

It has been shown that γ is related to the Z_s, which can be simply given as

$$\gamma E_{cBulk} = -[1 - (Z_s/Z_b)] \quad (5.1)$$

Considering the surface bond relaxation, γ has been revised as[27]

$$\gamma/E_{cBulk} = -[1 - (Z_s/Z_b)^{1/2}] \quad (5.2)$$

However, eq 5.2 underestimates the γ values compared with the experimental ones. Consequently, a correctional model has been developed through averaging eqs 5.1 and 5.2 as[27]

$$\gamma/E_{cBulk} = -[2 - (Z_s/Z_b) - (Z_s/Z_b)^{1/2}]/2 \quad (5.3)$$

The results from eq 5.3 were shown to be consistent with the experimental data for elemental metals.[27] Nevertheless, eq 5.2 has been shown to be more accurate than eq 5.3 when comparing the simulation results from DFT-GGA potential.[22] This is because the γ values from eq 5.2 are lower than the experimental data due to the absence of atomic repulsive potentials.[27] Meanwhile, the Kohn–Sham wave functions undergo a transition from propagating to evanescent character at the surface, which is also omitted from the GGA.[28] For instance, $\gamma_{111} = 1.32$ and $\gamma_{100} = 1.47$ J/m² obtained from the GGA functional for Cu[22] are consistent with those from eq 5.2 with $\gamma_{111} = 1.28$ and $\gamma_{100} = 1.54$ J/m². However, they are much lower than those from eq 5.3 with $\gamma_{111} = 1.83$ and $\gamma_{100} = 2.17$ J/m² and the available experimental value with $\gamma_{111} = 1.79$ J/m².[28] To implement the simulation results of E_{cBulk}, eq 5.2 is employed in this work.

With the two boundary conditions of $\delta \ll 1$ with $Z_s \approx Z_{sBulk} = 8$ and $\delta \rightarrow 1$, inserting eq 5.2 into eq 4, we determine that

$$E_c(n)/E_{cBulk} \approx 1 - (1 - \sqrt{6}/3)\delta \quad (6)$$

$$E_c(n)/E_{cBulk} \approx (Z_s/Z_b)^{1/2} \quad (7)$$

In addition, $(B_t - B_a)/B_t \equiv \delta(Z_b - Z_s)/Z_b$. Therefore

$$B_a/B_t = 1 - \delta(1 - Z_s/Z_b) \quad (8)$$

From eq 8, $B_a/B_t \approx Z_s/Z_b$ when $\delta \rightarrow 1$. When $\delta \rightarrow 0$, $B_a/B_t \rightarrow (B_a/B_t)^{1/2} \rightarrow 1$. Substituting these results into eq 7 permits $E_c(n)$ to be rewritten as the following equation
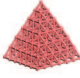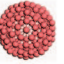
$$E_c(n)/E_{cBulk} \approx (B_a/B_t)^{1/2} \quad (9)$$

Eq 9 is applicable for any n as it complies with the boundary conditions of δ.

3. Results and Discussion

The simulated results $E_c(n)$ and the theoretical results n/B_t, δ, B_a, Z_s, and γ are listed in Table 1. In the case of the pyramid, $E_c(n) = 0, -1.42, -1.96, -2.24, -2.40, -2.50,$ and -2.58 eV/

TABLE 1: Obtained Results from the Computer Simulations and Theoretical Models for Cu Clusters[a]

Structure	l	Simulation	Theoretical model				
		$-E_e$	n/B_t	δ	B_a	Z_s	γ
Pyramids	1	0	1/6	1	0	0	3.12
	2	1.42	5/30	1	8	3.2	1.51
	3	1.96	14/84	1	36	5.14	1.08
	4	2.24	30/180	29/30	96	6.2	0.88
	5	2.40	55/330	10/11	200	6.8	0.77
	6	2.50	91/546	11/13	360	7.17	0.71
	7	2.58	140/840	11/14	588	7.42	0.67
Nanotubes	2	1.81	16/96	1	40	5	1.11
	3	2.06	24/144	1	68	5.67	0.98
	4	2.15	32/192	1	96	6	0.91
	5	2.20	40/240	1	124	6.2	0.88
	6	2.26	48/288	1	152	6.33	0.85
	7	2.26	56/336	1	180	6.42	0.84
	8	2.28	64/384	1	208	6.5	0.82
	9	2.29	72/432	1	236	6.56	0.81
	10	2.31	80/480	1	264	6.6	0.81
	11	2.32	88/528	1	292	6.64	0.8
	12	2.32	96/576	1	320	6.67	0.79
Nanorods	2×2	1.91	4/24	1	10	5	1.11
	3×3	2.38	9/54	8/9	32	6.5	0.82
	4×4	2.57	16/96	3/4	66	7	0.74
	5×5	2.69	25/150	16/25	112	7.25	0.69
	6×6	2.76	36/216	5/9	170	7.4	0.67
	7×7	2.82	49/294	24/49	240	7.5	0.66
	8×8	2.86	64/384	7/16	322	7.57	0.64
Films	2	2.58	8/48	1	32	8	0.57
	3	2.76	12/72	2/3	56	8	0.57
	4	2.85	16/96	1/2	80	8	0.57
	5	2.91	20/120	2/5	104	8	0.57
	6	2.95	24/144	1/3	128	8	0.57
	7	2.98	28/168	2/7	152	8	0.57
	8	3.00	32/192	1/4	176	8	0.57
	9	3.01	36/216	2/9	200	8	0.57
	10	3.02	40/240	1/5	224	8	0.57
	11	3.04	44/264	2/11	248	8	0.57
	12	3.04	48/288	1/6	272	8	0.57
Icosahedron	2	1.96	13/78	12/13	42	6	0.91
	3	2.54	55/330	42/55	234	7.43	0.66
	4	2.71	147/882	92/147	696	7.96	0.58

[a] E_c in eV/atom is derived from the DFT calculations. All the rest of the parameters are achieved from the theoretical models, where B_t, B_a, and Z_s are determined by eq 2, eq 3.a, and eq 3.b, respectively. δ is the surface/volume ratio, and γ in eV/atom is calculated in terms of Z_s and eq 5.2.

atom when $1 \leq l \leq 7$, respectively. Generally, a cluster with lower E_c has higher stability. Since $\delta \rightarrow 1$, the cluster possesses a higher E_c and therefore is in a less stable state. For the nanotube, $\delta \equiv 1$ and $E_c(n)$ ranges from -1.81 to -2.32 eV/atom because Z_s increases as l increases. The stability is improved as l increases with increasing Z_f. The atomic distance D at the end of the nanotube contracts after relaxation. Considering Cu96 as an example, $D = 2.49$ Å for inner atoms with $Z_f = 6$, and $D = 2.45$ Å for atoms at the end with $Z_e = 4$. Therefore, a contraction of ~1.4% is anticipated. For the nanorods, $-1.91 > E_c > -2.86$ eV/atom, the relaxed atoms on the edge move toward the cluster center resulting in a displacement of ~2.40–2.90%.[29] The high stability of the nanorod is partly related to the definition of l (while the length of the nanorod is infinite). As a result, the films are the most stable structure due to its smallest δ and Z_s values among the five structures. $-2.58 > E_c > -3.04$ eV/atom, and E_c tends to $E_{cBulk} = -3.12$ eV/atom as n increases. In the case of icosahedra,

Size and Structural Dependence of E_c in Cu

J. Phys. Chem. C, Vol. 112, No. 48, 2008 **18843**
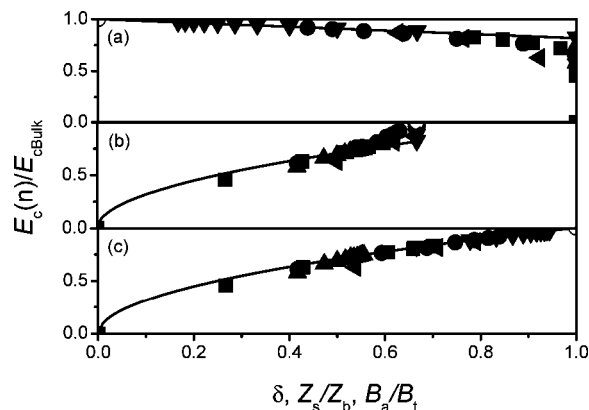
Figure 2. $E_c(n)/E_{cBulk}$ as functions of δ, (a), Z_s/Z_b (b), and B_a/B_t (c) for the simulated clusters. ■, ▲, ●,▼, and solid triangle pointing left are used to denote pyramids, nanotubes, nanorods, films, and icosahedrons, respectively. ○ is used to denote when $E_c(n\rightarrow\infty)/E_{cBulk} = 1$. The solid curves are separately determined by eqs 6, 7, and 9 where the related parameters are shown in Table 1 with the simulated E_{cBulk} = −3.12 eV/atom.

$E_c(n) = -1.96, -2.54$, and -2.71 when $n = 13, 55$, and 147, respectively. We render a comparison between the icosahedron and the pyramid here since both of them are 0-dimensional clusters. It is readily seen from Table 1 that the icosahedron has larger B_a and Z_s values but lower δ and γ values for a given n. Thus, the icosahedron is more stable than the pyramid. On the other hand, an inverse conclusion can be achieved by comparing the parameters between the icosahedron and the 1-dimensional nanotube. As a result, $E_{cNanotube} > E_{cPyramid} > E_{cIcosahedron} > E_{cNanorod} > E_{cFilm}$ for a given n. It should be noted that for a common n the structures of the pyramids and nanotubes are of significantly higher energy than the remaining structures. The most active nanotube has the biggest δ and the smallest Z_s, while the film is in reverse among the five structures.

Figure 2 shows $E_c(n)/E_{cBulk}$ as functions of δ, Z_s/Z_b, and B_a/B_t, respectively, for the five structures in terms of eqs 6, 7, and 9. When δ is small enough or n is large enough, the macroscopic rule of eq 6 is valid, which confers that only a small percentage of atoms are located on the surface, as shown in Figure 2a. Since almost all of the atoms are located on the surface when $\delta\rightarrow1$, the relative energetic differences between distinct structures can only be identified by Z_s/Z_b in light of eq 7 as shown in Figure 2b. It is discernible that the largest value of Z_s/Z_b in Figure 2b is 2/3 due to the quasi-fcc nature of the structures. The significance of this finding is that even if all atoms are located on the surface of a structure Z_s continues to be structure-dependent. Figures 2a and 2b present simulation results that deviate slightly at the upper limit of their curves from both equations due to their diminished suitability as $\delta\rightarrow0$ ($n\rightarrow\infty$) and $\delta\rightarrow1$ ($n\rightarrow0$). However, when B_a/B_t is taken as a variant in eq 9, the model is in good agreement with the simulation results across the full size range of n, as shown in Figure 2c. This is because B_a/B_t reflects the actual value of $E_c(n)/E_{cBulk}$, whereas the other two quantities do so indirectly.

The above continuous $E_c(n)/E_{cBulk}$ functions imply that if a structure remains constant the corresponding $E_c(n)/E_{cBulk}$ function depends only on the surface bond deficit, which is a continuous function of n. The observed fluctuation of $E_c(n < n_c)$ in the literature or quantum effect of the $E_c(n < n_c)$ function[3,11−16] is induced not by the change of n but by the corresponding structural changes due to the requirement of minimum energetic level for the total system. This can be exemplified by the case of Cu clusters. It has been shown that

the shape of the quasicrystalline icosahedron is more spherical than other 0-dimensional structures, and thus it can be a favorable structure with the lowest $\gamma(n)$ values.[13] However, since the multiply twinned icosahedron is highly symmetric, it might not be perfectly packed at some n values, which leads to stabilization of other structures, such as truncated octahedron structure at $n = 38$ and 79 and truncated decahedron structure at $n = 75$ and 101. These structure transformations would induce the quantum effect of E_c function, while their size variation effect is quite limited since $\delta\rightarrow1$ for all these small size clusters.

To understand the corresponding electronic changes, the partial density of states (PDOS) of the nanorods with different n and that of the bulk Cu as examples are determined and shown in Figure 3. The Fermi energy E_F is set to zero in our PDOS plots, which is defined as the energy at which half of the possible energy levels in the band are occupied by electrons in terms of the Fermi−Dirac statistics.[6] The 3d and 4s orbitals of Cu and their sum states are depicted therein. The two main peaks around −1.49 and −2.45 eV of 2 × 2 shown in Figure 3a are almost exclusively contributed by the Cu-3d orbital. The next peak at −4.02 eV is overlapped by the Cu-3d and Cu-4s orbitals, while the lowest energy band around −5.83∼−4.46 eV is fully occupied by the Cu-4s orbital. In comparison with the DOS of a 2 × 2 nanorod, the main peak of 3 × 3 has shifted lower in energy by ∼0.17 eV, and the intensity decreases from 6.85 to 6.53 states/eV (see Figure 3b). In addition, an evident new peak appears at −3.55 eV in Figure 3b, which is predominately occupied by the 3d state. Similarly, the electron orbitals shift toward lower energies, and the intensity of the bands decreases in sequence from Figure 3c to 3h. The above distribution of PDOS demonstrates that $E_{cNanotube}(n)$ decreases as n increases. PDOS of the other four structures of pyramids, icosahedron, nanotubes, and films are expected to show a trend similar to that observed in Figure 3. As shown in the inset plot in Figure 3h, our bulk DOS agrees perfectly with the one from a quite recent literature,[30] which was obtained by the GGA functional with Perdew−Wang parametrization. The pronounced closed 3d peak structure can be seen in the bulk PDOS, where two intensity peaks located at −1.68 and −2.82 eV can be found below the E_F. This confirms the validity of our electronic calculations. From the PDOS plots, the bands of the nanotube with smaller size are more close to the E_F. In addition, it is evident that their intensities are stronger and their bands are more localized in comparison with those of larger size clusters. These suggest that small clusters are more "eager" to lose charges since they are more chemically active. Therefore, smaller clusters represent stronger deoxidization ability and thus should have more metallic characters than the large ones.

The structure-dependent DOS plots of the nanotube ($n = 56$), pyramid ($n = 55$), icosahedron ($n = 55$), nanorod ($n = 49$), and film ($n = 48$) with similar n values are presented in Figure 4. Of these five structures, the main peak of the nanotube of DOS is closest to the E_F, as shown in Figure 4a. Comparing Figures 4b and 4c, although the main peaks of both the pyramid and the icosahderon are quite similar, the latter should be more stable because it has more evident peaks at the lower energy range. In Figure 4d, the states of the nanorod are predominantly situated toward lower energies and shown to peak at ∼−1.87 eV. Comparing Figure 4e with Figure 4f, the band of film atoms is narrowed with respect to that of a bulk atom, which is due to the reduction of the number of neighbors of surface atoms, and thus the band center gets closer to the E_F.[31] Among the five
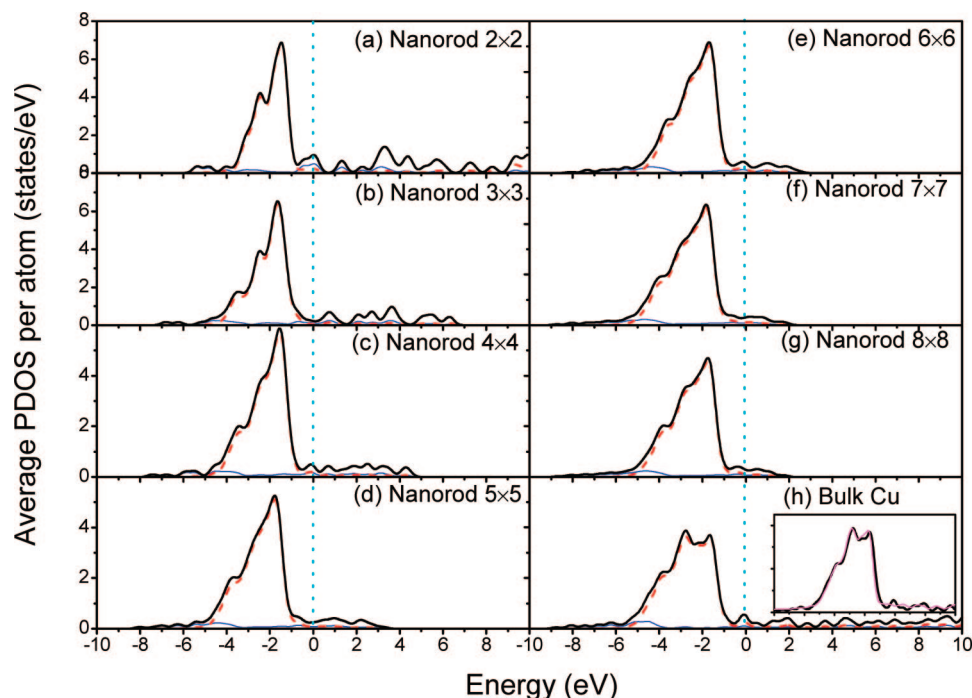
Figure 3. Size-dependent PDOS plots for Cu nanorods with different sizes: (a) 2 × 2, (b) 3 × 3, (c) 4 × 4, (d) 5 × 5, (e) 6 × 6, (f) 7 × 7, (g) 8 × 8, and (h) the bulk material. The solid, dashed, and thin solid lines indicate the sum, 3d, and 4s states of Cu, respectively. The Fermi level is set to zero and indicated by a dotted line. In addition, the inset plot in (h) compares our bulk DOS (shown by thick line) with other simulation results (shown by thin line) from ref 30.
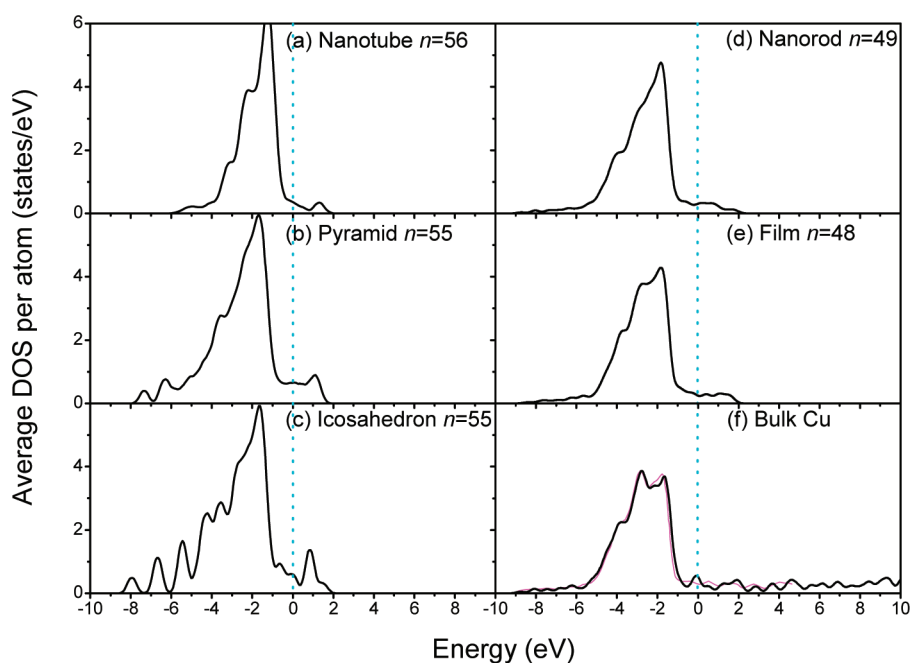
Figure 4. Structure-dependent DOS plots of Cu clusters: (a) a nanotube with $n = 56$, (b) a pyramid with $n = 55$, (c) an icosahedron with $n = 55$, (d) a nanorod with $n = 49$, (e) a film with $n = 48$, and (f) the bulk material, where another bulk result[30] is also depicted by the thin line to render a comparison. The Fermi level is set to zero and indicated by a dotted line.

reviewed structures, the DOS of the film demonstrates the greatest tendency toward lower energies, whereas the DOS of the nanotube tends toward the highest energies. Therefore, the order of $E_{cNanotube} > E_{cPyramid} > E_{cIcosahedron} > E_{cNanorod} > E_{cFilm}$ is justified.

4. Conclusions

The $E_c(n < n_c)/E_{cBulk}$ functions of five different structures of Cu clusters were determined by theoretical modeling and computer simulation. It is found that $E_c(n < n_c)/E_{cBulk}$, being similar to $E_c(n > n_c)/E_{cBulk}$, is a monotonic function of B_a/B_t at any n as long as the geometry of the considered structures remains constant. This phenomenon is also applicable to each of the structures irrespective of their geometrical differences. These findings for the continuous $E_c(n < n_c)$ functions are supported by DOS plots. These results suggest that the quantum effect of the $E_c(n < n_c)$ function is induced by structural changes, not by size changes.

Size and Structural Dependence of E_c in Cu

J. Phys. Chem. C, Vol. 112, No. 48, 2008 **18845**

References and Notes

(1) Wales, D. J. *Energy Landscapes with Applications to Clusters, Biomolecules and Glasses*; Cambridge University: Cambridge, England, 2003.

(2) Yang, M.; Jackson, K. A.; Koehler, C.; Frauenheim, T.; Jellinek, J. *J. Chem. Phys.* **2006**, *124*, 024308.

(3) Guvelioglu, G. H.; Ma, P.; He, X.; Forrey, R. C.; Cheng, H. *Phys. Rev. B* **2006**, *73*, 155436.

(4) Sun, C. Q. *Prog. Solid State Chem.* **2007**, *35*, 1.

(5) Guisbiers, G.; Wautelet, M. *Nanotechnology* **2006**, *17*, 2008.

(6) Askeland, D. R.; Phulé, P. P. *The Science and Engineering of Materials*, 4th ed.; Thomson Brooks/Cole: Pacific Grove, CA, 2004.

(7) Kim, H. K.; Huh, S. H.; Park, J. W.; Jeong, J. W.; Lee, G. H. *Chem. Phys. Lett.* **2002**, *354*, 165.

(8) Jiang, Q.; Li, J. C.; Chi, B. Q. *Chem. Phys. Lett.* **2002**, *366*, 551.

(9) Qi, W. H.; Wang, M. P.; Zhou, M.; Shen, X. Q.; Zhang, X. F. *J. Phys. Chem. Solids* **2006**, *67*, 851.

(10) Yang, C. C.; Jiang, Q. *Acta Mater.* **2005**, *53*, 3305.

(11) Yang, C. C.; Li, S. *Phys. Rev. B* **2007**, *75*, 165413.

(12) Fernández, E. M.; Soler, J. M.; Garzón, I. L.; Balbás, L. C. *Phys. Rev. B* **2004**, *70*, 165403.

(13) Grigoryan, V. G.; Alamanova, D.; Springborg, M. *Phys. Rev. B* **2006**, *73*, 115415.

(14) Alamanova, D.; Grigoryan, V. G.; Springborg, M. *J. Phys. Chem. C* **2007**, *111*, 12577.

(15) Li, X. B.; Wang, H. Y.; Yang, X. D.; Zhu, Z. H.; Tang, Y. J. *J. Chem. Phys.* **2007**, *126*, 084505.

(16) Schmidt, M.; Haberland, H. *CR Phys.* **2002**, *3*, 327.

(17) Delley, B. *J. Chem. Phys.* **1990**, *92*, 508.

(18) Delley, B. *J. Chem. Phys.* **2000**, *113*, 7756.

(19) Hammer, B.; Hansen, L. B.; Nørskov, J. K. *Phys. Rev. B* **1999**, *59*, 7413.

(20) Zhang, Y.; Yang, W. *Phys. Rev. Lett.* **1998**, *80*, 890.

(21) Delley, B. *Phys. Rev. B* **2002**, *66*, 155125.

(22) Swart, J. C. W.; van Helden, P.; van Steen, E. *J. Phys. Chem. C* **2007**, *111*, 4998.

(23) Qi, W. H.; Wang, M. P.; Xu, G. Y. *Chem. Phys. Lett.* **2003**, *372*, 632.

(24) Pawluk, T.; Hirata, Y.; Wang, L. *J. Phys. Chem. B* **2005**, *109*, 20817.

(25) Baletto, F.; Ferrando, R.; Fortunelli, A.; Montalenti, F.; Mottet, C. *J. Chem. Phys.* **2002**, *116*, 3856.

(26) Baletto, F.; Ferrando, R. *Rev. Mod. Phys.* **2005**, *77*, 371.

(27) Jiang, Q.; Lu, H. M.; Zhao, M. *J. Phys.: Condens. Matter* **2004**, *16*, 521, and references therein.

(28) Mattsson, A. E.; Kohn, W. *J. Chem. Phys.* **2001**, *115*, 3441.

(29) Liu, W.; Zhu, Y. F.; Lian, J. S.; Jiang, Q. *J. Phys. Chem. C* **2007**, *111*, 1005.

(30) Shang, J. X.; Zhao, X. D.; Lu, S.; Zhang, Y. *J. Phys.: Condens. Matter* **2008**, *20*, 135001.

(31) Lopez, N.; Nørskov, J. K. *Surf. Sci.* **2001**, *477*, 59.